

## Stability of the 1144 phase in iron pnictides

B. Q. Song, Manh Cuong Nguyen, C. Z. Wang, and K. M. Ho

Ames Laboratory, U.S. Department of Energy and Department of Physics and Astronomy, Iowa State University, Ames, Iowa 50011, USA

 (Received 7 April 2017; revised manuscript received 7 December 2017; published 14 March 2018)

A series of iron arsenides (e.g.,  $\text{CaRbFe}_4\text{As}_4$ ,  $\text{SrCsFe}_4\text{As}_4$ ) have been discovered recently, and have provoked a rise in superconductor searches in a different phase, known as the 1144 phase. For the presence of various chemical substitutions, it is believed that more 1144 compounds remain to be discovered. In this work, we perform general model analysis as well as scenario calculation on a basis of density functional theory to investigate phase stability in a variety of compounds. We predict that the 1144-type phase could be stabilized in  $\text{EuKFe}_4\text{As}_4$ ,  $\text{EuRbFe}_4\text{As}_4$ ,  $\text{EuCsFe}_4\text{As}_4$ ,  $\text{CaCsFe}_4\text{P}_4$ ,  $\text{SrCsFe}_4\text{P}_4$ ,  $\text{BaCsFe}_4\text{P}_4$ ,  $\text{InCaFe}_4\text{As}_4$ ,  $\text{InSrFe}_4\text{As}_4$ , etc. Remarkably, it involves rare earths, trivalence elements (e.g., indium) and iron phosphides, which greatly expands the range of its existence and suggests a promising prospect for experimental synthesis. In addition, we find that the formation of many random doping compounds (e.g.,  $\text{Ba}_{0.5}\text{Cs}_{0.5}\text{Fe}_2\text{As}_2$ ,  $\text{Ba}_{0.5}\text{Rb}_{0.5}\text{Fe}_2\text{As}_2$ ) is driven by entropy and could be annealed to a 1144-type phase. Eventually, we plot a phase diagram about two structural factors  $\Delta a$  and  $\Delta c$ , giving a bird's-eye view of stability of various 1144 compounds.

DOI: [10.1103/PhysRevB.97.094105](https://doi.org/10.1103/PhysRevB.97.094105)

### I. INTRODUCTION

Searching for superconductors (SC) has been a persistent hot issue in condensed-matter physics and material science [1]. Recently, a superconducting phase called 1144 (Fig. 1) was discovered inspiring a new tide of the search for superconductors [2–11].

In the 1144 phase, for instance,  $\text{CaKFe}_4\text{As}_4$  has the same chemical composition as the 50%-doped 122 phase. But distinct from random doping [12–19], it is structurally ordered with Ca and K occupying alternative cation layers. Given this feature, one is enabled to add electrons or holes without triggering the disorder effect. In that sense, the 1144 phase provides a different dimension for manipulation of material properties. It also inspires study of disorder-free superconducting materials beyond 1144 compounds (e.g.,  $\text{RbGd}_2\text{Fe}_4\text{As}_4\text{O}_2$ ,  $\text{KCa}_2\text{Fe}_4\text{As}_4\text{F}_2$ , etc.) [20].

The 1144 phase has previously been discovered in several different iron arsenides,  $XY\text{Fe}_4\text{As}_4$ , with cations  $X$  and  $Y$  being alkali metals (IA group) or alkaline-earth elements (IIA group) [2,5–10]. With these compounds synthesized, people start to wonder whether more 1144 structures could be stabilized. The main challenge arises from the fact that the 122 phase strongly competes with the desired 1144 phase. A phase diagram is proposed [2] to describe the relative stability of the two competing phases in iron arsenides. However, applicability of the phase diagram beyond iron arsenides is unclear yet. In this work, we investigate a series of unexplored systems and find that this phase could be stabilized in (i) iron-phosphide  $XY\text{Fe}_4\text{P}_4$ , (ii) Eu-contained 1144 iron arsenide  $\text{EuXFe}_4\text{As}_4$ , (iii) indium-contained 1144 compounds  $\text{InXFe}_4\text{As}_4$ . In addition, we find that the formation of the 122 solution phase for many compounds is driven by entropy, which means a phase transition to the 1144 phase could occur through an annealing process. By studying these systems, we are able to plot a generalized phase diagram, presenting a bird's-eye view of the stability of various 1144 materials.

The rest of work is organized as follows. Section II explains the methodology in estimating free energy. In Sec. III A, we analyze the general mechanism for stabilizing the 1144 phase. In each of the next subsections, we discuss the stability of 1144 structures sorted by chemical compositions: in Sec. III B the 1144  $XY\text{Fe}_4\text{As}_4$  with  $X$  and  $Y$  from IA or IIA groups; in Sec. III C, the rare-earth contained 1144 structure; in Sec. III D the 1144 iron phosphides; in Sec. III E the indium-contained 1144 structure. In Sec. III F, we will revisit the phase diagram and develop a generalized one.

### II. MODELING AND CALCULATION METHODS

The 1144 phase competes with the 122 solution phase during crystallization [2]. The 122 solution phase specifically means the random doping phase, for instance  $\text{Ca}_{0.5}\text{Na}_{0.5}\text{Fe}_2\text{As}_2$ , and it will be referred to as the 122(s) phase in this context. The relative stability of the two phases is characterized by the Gibbs free energy difference:

$$\Delta G(T) = G_{122(s)} - G_{1144} = \Delta H - S_{\text{conf}}T + \Delta E_0 - \Delta S_{\text{vib}}T, \quad (1)$$

where  $H$  is the enthalpy,  $S_{\text{conf}}$  is the configuration entropy,  $E_0$  is the zero-point energy, and  $S_{\text{vib}}$  is the vibrational entropy. Positive  $\Delta G$  is defined as favoring the 1144 phase.

At zero pressure, the enthalpy  $\Delta H$  is just the energy difference, which can be estimated by density functional theory (DFT). For the 122(s) phase, it involves a sum of random configurations, which is unfeasible for supercell modeling. Thus we adopt an ideal solution approximation:

$$E_{122(s)} = x E_{X\text{Fe}_2\text{As}_2} + (1-x) E_{Y\text{Fe}_2\text{As}_2}, \quad (2)$$

where  $x$  is the concentration of  $X$  cations, which is 1/2 in our case.  $E_{X\text{Fe}_2\text{As}_2}$  and  $E_{Y\text{Fe}_2\text{As}_2}$  are energies of two pure 122 phases.

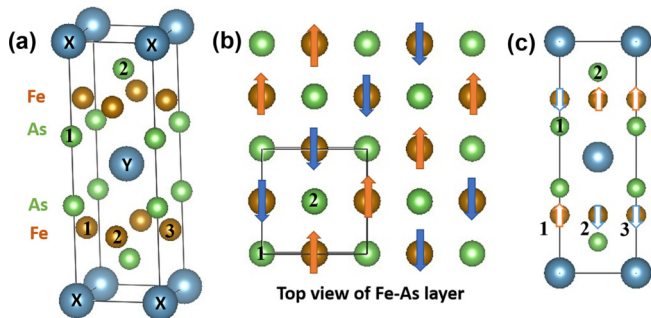


FIG. 1. (a) Crystal structure of 122/1144. If the  $X$  and  $Y$  sites are occupied by the same type of atoms, one obtains the 122 phase  $X\text{Fe}_2\text{As}_2$ ; if  $X$  and  $Y$  sites are occupied by different atoms, one obtains the 1144 phase  $XY\text{Fe}_4\text{As}_4$ . (b) Top view of a single Fe-As layer. The Fe atoms locate in a plane, forming a square lattice. Two types of arsenic atoms located above and below the Fe plane, as designated by 1 and 2. The arrows indicate spin directions, which are stripelike AFM. (c) Interlayer magnetic structure. Two neighboring Fe-As with AFM coupling.

For the 1144 phase,  $S_{\text{conf}}$  is zero. For the 122( $s$ ) phase, it (per unit cell) can be estimated by

$$S_{\text{conf}} = 2k_B[x \ln x + (1-x) \ln(1-x)]. \quad (3)$$

Each tetragonal unit cell contains two primitive unit cells, leading to the prefactor 2. In this case,  $S_{\text{conf}}$  is a constant 0.011 96 meV/(atom K).

Calculations of zero-point energy and vibration entropy are implemented by the code *phonopy* under a harmonic approximation [21]. To account for the solution phase, we made a similar approximation as made for enthalpy:

$$S_{\text{vib}}^{122(s)} = x S_{\text{vib}}^{X\text{Fe}_2\text{As}_2} + (1-x) S_{\text{vib}}^{Y\text{Fe}_2\text{As}_2}, \quad (4)$$

as well as for zero-point energy:

$$E_0^{122(s)} = x E_0^{X\text{Fe}_2\text{As}_2} + (1-x) E_0^{Y\text{Fe}_2\text{As}_2}. \quad (5)$$

TABLE II. Lattice constants and enthalpy difference of the 1144 phase with various IA-IIA combinations. The left portion lists 1144-stable combinations; the right portion lists 122( $s$ )-stable combinations. (The enthalpy difference estimated based on experimental and calculated lattice constants are listed in Expt.-latt and Calc.-latt columns respectively.)

1144	Lattice (Å)		$\Delta H$ (meV/atom)		122( $s$ )	Lattice (Å)		$\Delta H$ (meV/atom)
	Expt.	Calc.	Expt.-latt.	Calc.-latt.		Calc.	Calc.-latt.	
BaCsFe <sub>4</sub> As <sub>4</sub>	$a = 3.9272$ $c = 14.1346$	$a = 3.8618$ $c = 14.2802$	4.435	6.187	BaRbFe <sub>4</sub> As <sub>4</sub>	$a = 3.8512$ $c = 13.9903$	5.035	
SrCsFe <sub>4</sub> As <sub>4</sub>	$a = 3.9101$ $c = 13.7293$	$a = 3.8509$ $c = 13.8921$	9.270	10.200	BaKFe <sub>4</sub> As <sub>4</sub>	$a = 3.8480$ $c = 13.6245$	2.952	
SrRbFe <sub>4</sub> As <sub>4</sub>	$a = 3.8971$ $c = 13.4175$	$a = 3.8209$ $c = 13.6981$	9.064	10.125	BaNaFe <sub>4</sub> As <sub>4</sub>	$a = 3.8324$ $c = 12.8097$	-4.730	
CaCsFe <sub>4</sub> As <sub>4</sub>	$a = 3.8911$ $c = 13.4142$	$a = 3.8265$ $c = 13.6048$	14.205	13.809	SrKFe <sub>4</sub> As <sub>4</sub>	$a = 3.8187$ $c = 13.3285$	7.596	
CaRbFe <sub>4</sub> As <sub>4</sub>	$a = 3.87579$ $c = 13.1043$	$a = 3.7976$ $c = 13.4460$	14.912	15.698	SrNaFe <sub>4</sub> As <sub>4</sub>	$a = 3.7849$ $c = 12.8473$	1.932	
CaKFe <sub>4</sub> As <sub>4</sub>	$a = 3.8661$ $c = 12.8175$	$a = 3.7865$ $c = 13.1135$	12.378	13.585	CaNaFe <sub>4</sub> As <sub>4</sub>	$a = 3.9876$ $c = 11.7920$	2.876	

TABLE I. The lattice constants of eight known 122 iron arsenides  $X\text{Fe}_2\text{As}_2$ . The values in column Expt. are measured by experiment [18] and those in column Calc. are obtained from DFT calculation.

	Lattice (Å)		Lattice (Å)	
	Expt.	Calc.	Expt.	Calc.
Cs	$a = 3.8894$ $c = 15.0665$	$a = 3.8661$ $c = 15.1569$	Ba	$a = 3.9612$ $c = 13.0061$
Rb	$a = 3.8882$ $c = 14.5347$	$a = 3.8184$ $c = 14.5342$	Sr	$a = 3.9267$ $c = 12.3702$
K	$a = 3.8414$ $c = 13.8371$	$a = 3.7953$ $c = 13.9198$	Ca	$a = 3.9001$ $c = 11.6210$
Na	$a = 3.8091$ $c = 12.4413$	$a = 3.7521$ $c = 12.6661$	Eu	$a = 3.9062$ $c = 12.1247$

DFT calculation details are as below. All calculations are implemented by Vienna *ab initio* simulation package (VASP) [23]. It is performed based on Perdew-Burke-Ernzerhof (PBE) exchange-correlation functional [22]. The projected augmented wave (PAW) pseudopotential method [24] is employed. The minimum  $1 \times 1 \times 1$  tetragonal unit cell of  $XY\text{Fe}_4\text{As}_4$  is shown in Fig. 1(a). In calculating energy, we construct an enlarged  $2 \times 2 \times 1$  supercell to account for the stripe antiferromagnetic (AFM) ordering within the Fe-As layer [Figs 1(b) and 1(c)]. For the Eu-contained 1144 structure, there are some debates about the Fe-As magnetic ordering [25,26], which are mainly about the spin orientation angle with respect to the  $z$  axis. Nevertheless, the AFM feature is unambiguous. In calculating the force matrix needed for the computation of  $S_{\text{vib}}$ , we have created an enlarged  $3 \times 3 \times 1$  supercell for both 122 and 1144 phases. The lattice constants are chosen as the calculated values listed in Tables I and II. We turned off spins for affordable computational efforts in the phonon part.

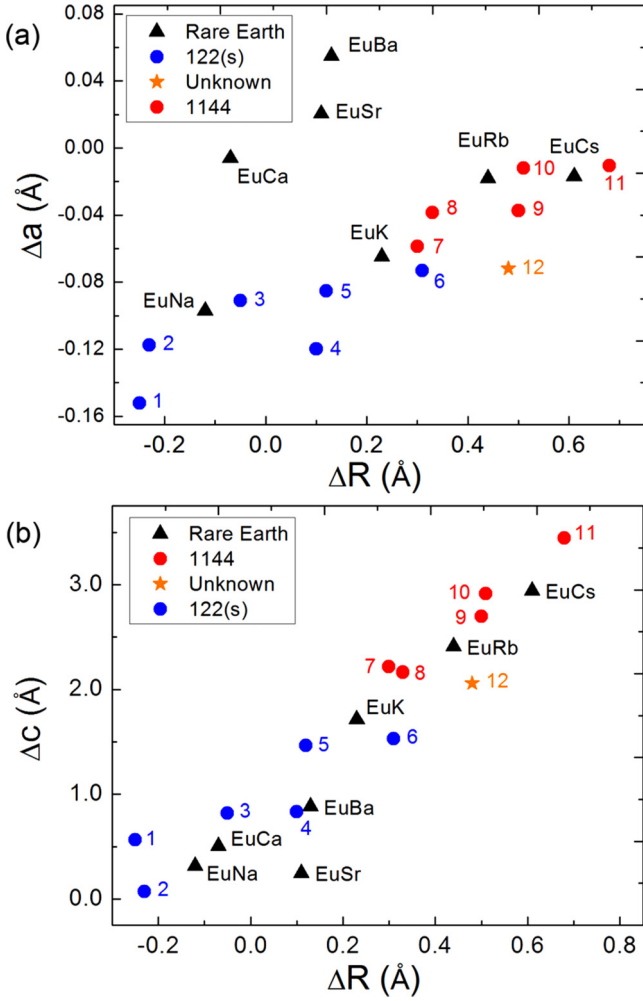


FIG. 2. (a) The 1144-122(s) phase diagram in Ref. [2]. We also add Eu-contained combinations into the graph (black triangles). Each point represents a particular  $X$ - $Y$  combination. The parameter is defined as  $\Delta a = a_{X\text{Fe}_2\text{As}_2} - a_{Y\text{Fe}_2\text{As}_2}$ ,  $\Delta c = c_{X\text{Fe}_2\text{As}_2} - c_{Y\text{Fe}_2\text{As}_2}$ , where  $a$  and  $c$  are the lattice constants of the tetragonal 122 unit cell. Note that, to plot this figure, one needs only to know the lattice for two 122 phases, and no need for the lattice of 1144 phase. The combinations that have resulted in the 1144 phase in experiment are colored in red, while the ones of 122(s) phase are in blue.  $\text{BaCsFe}_4\text{As}_4$  remains to be determined (shown as an orange star). It is clear that linear correlation does not hold between  $\Delta a$  and  $\Delta R$ . (b) The linear correlation  $\Delta c = \gamma \Delta R$ , where  $\gamma$  is about 4.0. The number notation for both (a) and (b) is 1-BaNa, 2-SrNa, 3-CaNa, 4-BaK, 5-SrK, 6-BaRb, 7-CaK, 8-SrRb, 9-SrCs, 10-CaRb, 11-CaCs, 12-BaCs.

### III. RESULTS AND DISCUSSION

#### A. Mechanism of 1144-122(s) phase stability

Before presenting numerical results, it seems beneficial to discuss the general mechanism of phase stability. It is observed that, for the iron arsenide, 1144-122(s) phase stability depends on two parameters [2]: the difference in lattice constant  $\Delta a$  and the difference in atomic radius  $\Delta R$ . Such dependence is demonstrated with a phase diagram [2], which is re-plotted in Fig. 2(a). Evidently, the 1144 phase will be stabilized with  $\Delta R > 0.4 \text{ \AA}$  and  $|\Delta a| < 0.07 \text{ \AA}$ , while the 122(s) phase locates

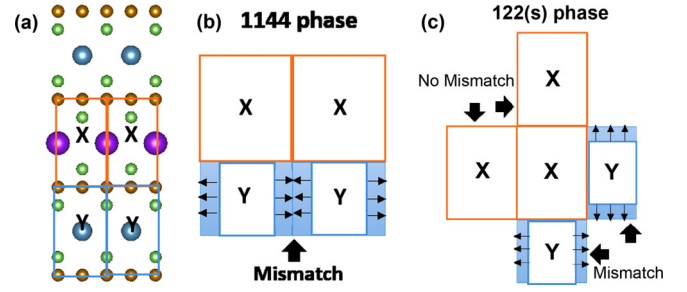


FIG. 3. (a) Schematics of 1144 structures. The  $X$  boxes (red) and (blue) are shorthand representation for building blocks. (b) For 1144 phase,  $X$  and  $Y$  boxes are in different layers, thus the mismatch only occurs in  $x$ - $y$  plane. (c) For 122(s) phase, mismatch occurs in both  $x$ - $y$  plane and  $z$  axis. The probability for mismatch to occur is  $1/2$  due to a random distribution of  $X$ - $Y$  boxes.

in  $\Delta R < 0.4 \text{ \AA}$  and  $|\Delta a| > 0.07 \text{ \AA}$ . However, its physical mechanism remains unexplained. For example, why does large  $\Delta R$  tend to stabilize the 1144 phase, while large  $\Delta a$  tends to stabilize the 122(s) phase? In addition, a phase diagram's applicability beyond iron arsenide is unclear yet. In this work, we suggest using  $\Delta c$  (the mismatch of lattice  $c$ ) to replace  $\Delta R$  as the new characterizing parameter. The parameter  $\Delta c$  will serve equally well as  $\Delta R$  for plotting the phase diagram, because  $\Delta c$  is linearly correlated with  $\Delta R$  ( $\Delta c \approx 4\Delta R$ ) as shown in Fig. 2(b). Making such a replacement will merely lead to a horizontal rescale of the original phase diagram. [Note that linear correlation does not hold between  $\Delta R$  and  $\Delta a$  as shown Fig. 2(a). In that sense  $\Delta a$  and  $\Delta c$  respond differently to  $\Delta R$ .] On the other hand,  $\Delta c$  is advantageous in explaining the mechanism with an elastic box picture as sketched below.

Imagine the  $X$  or  $Y$  atoms together with the surrounding Fe-As as an elastic box [Fig. 3(a)], whose energy will increase as the box is compressed or expanded. Suppose the stiffness for  $a$  and  $c$  is  $k_a$  and  $k_c$  ( $k_a > k_c$ ). Then the energy increase in the  $a$  and  $c$  axis per box is

$$\Delta E_a = n_a p_a \frac{1}{2} k_a (\Delta a)^2, \quad (6)$$

$$\Delta E_c = n_c p_c \frac{1}{2} k_c (\Delta c)^2. \quad (7)$$

$n_a$  and  $n_c$  are the neighborhood numbers. For both the 1144 and 122(s) phases,  $n_a = 1$  and  $n_c = 2$  (there are two interfaces on the top and bottom and four on the sides, but one interface is shared by two boxes).  $p_a$  and  $p_c$  are the probabilities for that sort of mismatch to occur. For the 1144 phase,  $p_a = p_c = 1$ . For the 122(s) phase with a random distribution of  $X$ - $Y$  boxes, the probability for the same or different cations occupying the neighborhood is equal [Fig. 3(c)]. Thus  $p_a = p_c = 1/2$ . In addition, the 1144 phase has heterocations in different layers, thus  $\Delta c = 0$  [Fig. 3(b)]. Then the energy difference for the two phases is

$$E^{1144} - E^{122(s)} = \frac{1}{4} k_a (\Delta a)^2 - \frac{1}{2} k_c (\Delta c)^2. \quad (8)$$

From an energy point of view, small  $\Delta a$  and large  $\Delta c$  tend to stabilize the 1144 phase, while the 122(s) phase is stabilized the other way. This is a pure size effect, independent of the nature of cations or skeleton layers. Therefore, it should be generally applied for the 1144-122(s) competition. In each of

the following sections, we will use the methodology outlined in Sec. II to test the mechanism. In Sec. III F, we provide a generalized phase diagram (Fig. 6) based on these calculations.

### B. 1144 with IA+IIA combination

Eight 122 iron arsenides  $X\text{Fe}_2\text{As}_2$  ( $X = \text{IA}$  or  $\text{IIA}$  group elements, or  $\text{Eu}$ ) have been found in experiment (listed in Table I). The 1144 phase could be obtained by combining two of these 122 compounds. In this section, we will discuss the  $X$ - $Y$  combinations of IA- or IIA-group elements, which could be further divided into three groups: IA+IIA, IA+IA, and IIA+IIA. The IA+IIA combinations have received the most attention due to the electron/hole doping attempts [2–6]. Thus we will first investigate this group and compare our calculation with experiment results, then move on to other combinations.

We have calculated enthalpy difference using both experimental and calculated lattice constants, labeled as Expt.-latt and Calc.-latt in Table II. For Expt.-latt, we fix the lattice constants to the experimental values and only relax the internal coordinates. For Calc.-latt, we relax both the internal coordinates and lattice constants. For most 122 compounds, the difference of experiment and calculation lattice constants are around 1%. The only exception is  $\text{CaFe}_2\text{As}_2$ ; it differs by 2.0% for  $a$  and 5.0% for  $c$ . Note that  $\text{CaFe}_2\text{As}_2$  is a special 122 compound, which is extremely sensitive to external pressure on its crystal structure [27]. The higher discrepancy might be a consequence of such complications. For 1144 compounds, such differences are about 2% or less.

There are 12 IA+IIA combinations, some of which have been found 1144 stable (e.g.,  $\text{CaKFe}_4\text{As}_4$ ,  $\text{CaRbFe}_4\text{As}_4$ ). Others appear to be 1144 unstable, showing the 122( $s$ ) phase [2]. The left portion of Table II lists 1144-stable compounds (except for  $\text{BaCsFe}_4\text{As}_4$ , whose phase remains undetermined). Our calculation illustrates that all these systems have positive  $\Delta H$ , which suggests a 1144 ground state at zero temperature. At finite temperature, we need to estimate the free energy as defined in Eq. (1). We plot the free energy vs temperature in Figs. 4(a)–4(e). For each compound, we have plotted two lines. The straight dashed line only includes the first two terms  $\Delta H$  and  $-S_{\text{conf}}T$ . The other line further includes the effect of zero-point energy and vibration entropy contribution. By comparing the two lines, we can see how the zero-point energy and phonons affect the phase stability for a specific compound. Before adding zero-point energy and phonons,  $\Delta G$  linearly decreases with temperature. Thus, at high enough temperature, 122( $s$ ) will eventually predominate. We can find the critical temperature for the phase transition ( $\Delta G = 0$ ), which is higher than 800 K for all these systems. After zero-point energy and phonons are added into consideration; the line is curved but the general trend stays the same, which suggests that the vibration entropy plays a relatively minor role in configuration entropy. The critical temperature changes as follows:  $\text{CaRb}$  (1314 K  $\rightarrow$  700 K),  $\text{CaCs}$  (1156 K  $\rightarrow$  830 K),  $\text{CaK}$  (1137 K  $\rightarrow$  780 K),  $\text{SrCs}$  (854 K  $\rightarrow$  1000+ K),  $\text{SrRb}$  (848 K  $\rightarrow$  630 K). Most of them have a decreased critical temperature, however, still well above the room temperature.  $\text{SrCsFe}_4\text{As}_4$  is an exception, whose critical temperature is substantially enhanced to greater than 1000 K. Nevertheless, adding vibration and zero-point energy does not change the conclusion qualitatively.

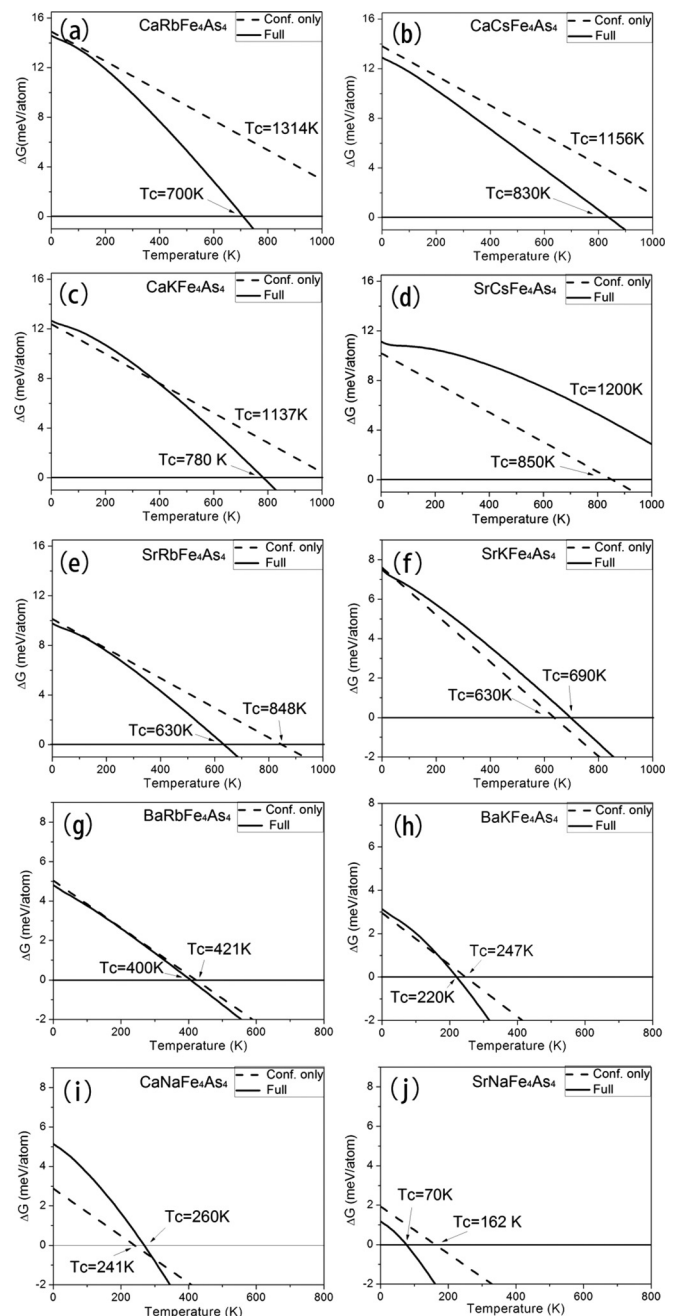


FIG. 4. The temperature dependence of  $\Delta G$ . The dashed line is for free energy with configuration entropy only. The solid line includes the effect of vibration entropy and zero-point energy. These curves are calculated with theoretical lattice constants. Two critical temperatures ( $\Delta G = 0$ ) are denoted for each compound. Positive  $\Delta G$  is defined as favor the 1144 phase.

The right portion of Table II lists 1144-unstable compounds. Most of them (except  $\text{BaNaFe}_4\text{As}_4$ ) show positive enthalpy, but  $\Delta H$  is substantially smaller than 1144-stable compounds, which means  $\Delta H$  will probably not suffice to maintain the 1144 phase at finite temperature and the 122( $s$ ) phase will be formed driven by entropy. The free energy is shown in Figs. 4(f)–4(i). In this case, vibration leads to a minor correction to the critical temperature:  $\text{SrNa}$  (162 K  $\rightarrow$  70 K),  $\text{BaK}$  (247 K  $\rightarrow$  220 K),  $\text{CaNa}$  (241 K  $\rightarrow$  260 K),  $\text{BaRb}$  (421 K

TABLE III. Lattice constants (obtained from DFT) and enthalpy difference of 1144 phase  $XYFe_4As_4$  with  $X$ - $Y$  combinations of IA+IA and IIA+IIA.

I+I	Lattice (Å)	$\Delta H$ (meV/atom)	II+II	Lattice (Å)	$\Delta H$ (meV/atom)
CsRb	$a = 3.8511$ $c = 14.8420$	-0.949	BaSr	$a = 3.8926$ $c = 12.9654$	-0.182
CsK	$a = 3.8195$ $c = 14.6174$	-0.162	BaCa	$a = 3.8602$ $c = 12.7393$	-0.626
CsNa	$a = 2.7973$ $c = 13.9261$	-0.759	SrCa	$a = 3.8294$ $c = 12.4775$	-0.664
RbK	$a = 3.8094$ $c = 14.2627$	0.784			
RbNa	$a = 3.7840$ $c = 13.6154$	1.226			
KNa	$a = 3.7703$ $c = 13.3331$	1.199			

→ 400 K), SrK (630 K → 690 K). SrNa, BaK, and CaNa show critical temperature lower than room temperature, and are thus hard to stabilize. BaRb is around room temperature, indicating a better stability. SrKFe<sub>4</sub>As<sub>4</sub> is recognized as the most promising one, which shows a critical temperature higher than 600 K and is even further enhanced when vibration is taken into consideration. In Fig. 2(b), the BaRb and SrK, located near the boundary of the 1144 and 122(s) phase, also suggest a chance to be stabilized.

The single crystal of CaKFe<sub>4</sub>As<sub>4</sub> has recently been synthesized [7–10]. One practical challenge is to avoid unwanted phases (mainly 122 phase) [7]. Growing a 1144 phase free of impurity sensitively depends on chemical composition and temperature control [7]. Thus, growing a high quality crystal requires a sufficiently high critical temperature, which allows a broad window to achieve the desired phase. CaRbFe<sub>4</sub>As<sub>4</sub> and CaCsFe<sub>4</sub>As<sub>4</sub> are showing critical temperatures similar to CaKFe<sub>4</sub>As<sub>4</sub>. Thus one can expect a comparable chance to obtain a single-crystalline 1144 phase. SrCsFe<sub>4</sub>As<sub>4</sub> shows an even better stability, as a phonon will substantially enhance the stability of the 1144 phase. For BaCsFe<sub>4</sub>As<sub>4</sub>, which phase it belongs to remains undetermined in experiment. Our calculation shows that a phonon will substantially decrease the stability of the 1144 phase (510 K → 200 K).

Next we will examine IA+IA and IIA+IIA combinations. Our result is listed in Table III. There are six combinations for IA+IA and three for IIA+IIA. We find that 1144 compounds have negative  $\Delta H$ . Even RbK, RbNa, and KNa have positive  $\Delta H$ ; the critical temperature is extremely low, which suggests the stability of the 1144 phase is poor in these compounds. If we examine the locations of these systems in the phase diagram, we will find they mainly locate in the off-diagonal region, i.e., the region with  $\Delta R < 0.4$  Å and  $|\Delta a| < 0.07$  Å.

### C. 1144 with rare earth

In this section, we discuss Eu-bearing 1144 phases. Fe-As does not form the 122 phase with rare-earth elements, while Eu is the only exception. We expect Eu is capable of forming

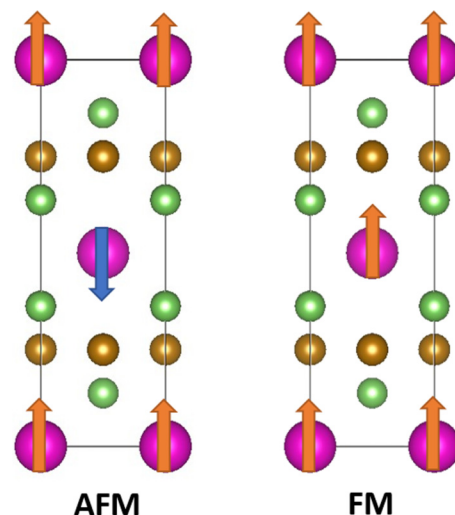


FIG. 5. The AFM and FM spin configurations of EuFe<sub>2</sub>As<sub>2</sub>. The spin in Fe-As layer is same as Fig. 1(b), but not explicitly shown in the graph. The magnetic moment on each Eu is about  $6.5\mu_B$  according to our calculations.

1144 phase iron arsenide in company with other main group elements. Unlike main group elements, Eu is magnetic with a local moment about  $5.9\mu_B$  [30]. Thus magnetism might play a role in phase stability. We use two types of PAW pseudopotentials in investigating phase stability. One considers the  $f$  electron as valence electrons; the other builds the  $f$  electron into the core, which is a routine way to cope with the inabilities of present DFT functional to describe the localized  $4f$  electrons.

With the first pseudopotential, one is able to account for Eu's magnetism: AFM or FM as shown in Fig. 5. The two configurations were found similar in energy [25,28] and AFM can be converted to FM by an external magnetic field, which suggests a weak AFM coupling between Eu layers [29]. Thus, for a more efficient calculation (AFM needs to double the unit cell), we consider FM configuration in investigation of the stability of EuXFe<sub>4</sub>As<sub>4</sub> structures. It predicts a magnetic moment of  $6.5\mu_B$  for Eu. For the second pseudopotential, Eu is nonmagnetic as the  $f$  electron is frozen into the core.

The formation enthalpies are listed in Table IV. For all Eu+IA combinations, the ground state is a 1144 structure at zero temperature. This is true for both pseudopotentials. Our calculation shows that the 1144 stability of EuCs and EuRb, comparatively, is better than EuK and EuNa. In Fig. 2(a), the phase diagram demonstrates EuCs and EuRb locating in the 1144 region, EuK is at the boundary, while EuNa is even further. Thus the phase diagram gives a consistent ranking of stability among these compounds. A non- $f$ -electron pseudopotential has provided the same conclusion, but a different formation enthalpy. In addition, polycrystallines of EuCsFe<sub>4</sub>As<sub>4</sub> and EuRbFe<sub>4</sub>As<sub>4</sub> have recently been synthesized [3,4,6]. The lattice constants are found to be  $a = 3.9002$  Å and  $c = 13.6285$  Å for EuCsFe<sub>4</sub>As<sub>4</sub> and  $a = 3.89$  Å  $c = 13.31$  Å for EuRbFe<sub>4</sub>As<sub>4</sub>. It seems a non- $f$ -electron pseudopotential provides a closer estimate of lattice constants. Nevertheless, our finding is verified by EuCsFe<sub>4</sub>As<sub>4</sub> and EuRbFe<sub>4</sub>As<sub>4</sub> being

TABLE IV. The lattice constants and enthalpy difference for Eu-bearing 1144 structures  $\text{EuXFe}_4\text{As}_4$ . It is obtained by DFT calculation with two different pseudopotentials. The pseudopotential with  $f$  electron built in the core is labeled by *non- $f$* .

	Lattice (Å)	$\Delta H$ (meV/atom)	Lattice (non- $f$ ) (Å)	$\Delta H$ (non- $f$ ) (meV/atom)
EuCs	$a = 3.8369$ $c = 13.7026$	9.914	$a = 3.8908$ $c = 13.4982$	4.848
EuRb	$a = 3.8017$ $c = 13.4911$	11.456	$a = 3.8763$ $c = 13.1503$	5.942
EuK	$a = 3.8132$ $c = 13.1216$	9.196	$a = 3.8361$ $c = 13.0232$	4.024
EuNa	$a = 3.7673$ $c = 12.4489$	4.581	$a = 3.8355$ $c = 12.1161$	2.090
EuBa	$a = 3.8822$ $c = 12.6882$	-1.871	$a = 3.9055$ $c = 12.6311$	-2.667
EuSr	$a = 3.8142$ $c = 12.6123$	-3.302	$a = 3.8659$ $c = 12.4614$	-4.913
EuCa	$a = 3.8201$ $c = 12.1892$	0.263	$a = 3.9010$ $c = 11.7391$	1.450

stable at room temperature. We further predict  $\text{EuKFe}_4\text{As}_4$  and  $\text{EuNaFe}_4\text{As}_4$ , which remains to be tested.

#### D. 1144 of iron phosphides

In this section, we discuss iron phosphide 1144 structures. Similar to iron arsenides, pure iron phosphides (e.g.,  $\text{CaFe}_2\text{P}_2$  [31],  $\text{LaFe}_2\text{P}_2$  [32]) do not show superconductivity. But replacing Fe with Ru (e.g.,  $\text{LaRu}_2\text{P}_2$  [33]) will induce superconductivity at low temperature. For structural stability, it is interesting to check whether the parameters  $\Delta a$  and  $\Delta c$  can equally characterize the 1144 phase stability in iron phosphides, where the skeleton Fe-As layer becomes Fe-P layers. We discuss four 122 iron phosphides:  $\text{BaFe}_2\text{P}_2$ ,  $\text{SrFe}_2\text{P}_2$ ,  $\text{CaFe}_2\text{P}_2$ , and  $\text{CsFe}_2\text{P}_2$ , which have been discovered in experiment. Then we proceed to study three unknown 1144 systems, which include  $\text{BaCsFe}_4\text{P}_4$ ,  $\text{SrCsFe}_4\text{P}_4$ , and  $\text{CaCsFe}_4\text{P}_4$ .

The method we used is similar as for iron arsenide in Secs. III B and III C. The lattice constants and enthalpy difference are listed in Table V. Note that the lattice constants are generally smaller compared with their counterparts in iron arsenide. All three 1144 structures show positive  $\Delta H$ , implying a stable 1144 phase. That is particularly true for  $\text{CaCsFe}_4\text{P}_4$ .

#### E. 1144 with IIIA elements

In this section, the possibility of building IIIA elements into 1144 structures is studied. The 1144 phase has been discovered with IA or IIA elements, while no IIIA-element-contained 1144 structures have been reported to date. That is possibly because the IIIA element has an electronegativity about 1.7–1.8, apparently higher than IA or IIA groups. Our idea is to use a partner element from IA or IIA to help IIIA form the 1144 phase. In fact, this idea also applies to other trivalence electrons (e.g., Y, La, etc.) to form the 1144- or 122-type structures.

TABLE V. Lattice constants and enthalpy of several 122  $\text{XFe}_2\text{P}_2$  (left portion) and 1144  $\text{XYFe}_4\text{P}_4$  (right portion). The lattices of 122 iron phosphides are cited from the database *Springer Materials* online. The 1144 phase has not been prepared and the lattice is obtained from calculation.

122	Lattice (Å)		1144	Lattice (Å)	$\Delta H$ (meV/atom)
	Expt.	Calc.			
Ba	$a = 3.8400$ $c = 12.4420$	$a = 3.7597$ $c = 12.8189$	BaCs	$a = 3.7597$ $c = 3.6890$	7.078
Sr	$a = 3.8250$ $c = 11.6120$	$a = 3.7225$ $c = 12.1068$	SrCs	$a = 3.6890$ $c = 13.3847$	8.865
Ca	$a = 3.8550$ $c = 9.9850$	$a = 3.6878$ $c = 11.4919$	CaCs	$a = 3.7186$ $c = 13.0452$	14.839
Cs	$a = 3.8258$ $c = 14.2960$	$a = 3.7346$ $c = 14.6846$			

In addition, a relatively low melting point (e.g., lower than 1200 K) is easier for applicability of solution growth [5,7]. Thus, indium (In) with a melting point about 156 °C is chosen. Recently, several new iron SCs, called 12442 structures, have been synthesized [34,35], which inspires us to study the 1144 compounds.

Note that indium does not form a 122 phase with Fe and As, but will decompose into  $\text{Fe}_2\text{As}$  and  $\text{InAs}$ . Thus, we define the enthalpy difference  $\Delta H$ :

$$\Delta H = \frac{1}{2}E_{\text{XFe}_2\text{As}_2} + E_{\text{Fe}_2\text{As}} + E_{\text{InAs}} - E_{\text{InXFe}_4\text{As}_4}. \quad (9)$$

The factor 1/2 comes from the fact that each unit cell is composed of two formula units. The energy of  $\text{Fe}_2\text{As}$  is estimated based on an AFM coupling [36]. In this case, the enthalpy difference shows stability of the 1144 phase against decomposition. In our calculation, we find the best partner for In is K among other alkali metals and Ca is the best among alkaline-earth elements. It also indicates that alkaline-earth elements are better than alkali metals; smaller atoms are better than larger atoms. The apparent correlation between the stability and atomic size implies the atomic size is still an important factor. As a reference, we also calculate the energy of  $\text{InFe}_2\text{As}_2$ , which shows a negative  $\Delta H$ , consistent with the fact that the 122 phase  $\text{InFe}_2\text{As}_2$  is unstable.

#### F. Generalized phase diagram

Finally, we are able to plot a generalized phase diagram [Fig. 6(a)], containing all the compounds investigated above. Several changes have been made on the original one [Fig. 2(a)]. First, substitute  $\Delta R$  by  $\Delta c$ , then the stability of 1144 and 122(s) phases can be understood with a simple elastic box picture. Second, we discard the sign of  $\Delta c$  and only take its absolute value, because the sign seems not significant for characterizing the interbox mismatch.  $\Delta a$  is set negative to make the data point distribution look similar to the original phase diagram. Third, to make the phase diagram self-consistent, the lattice constants are all based on calculated values instead of experimental values. As we show, the calculated values are very close to experimental values.

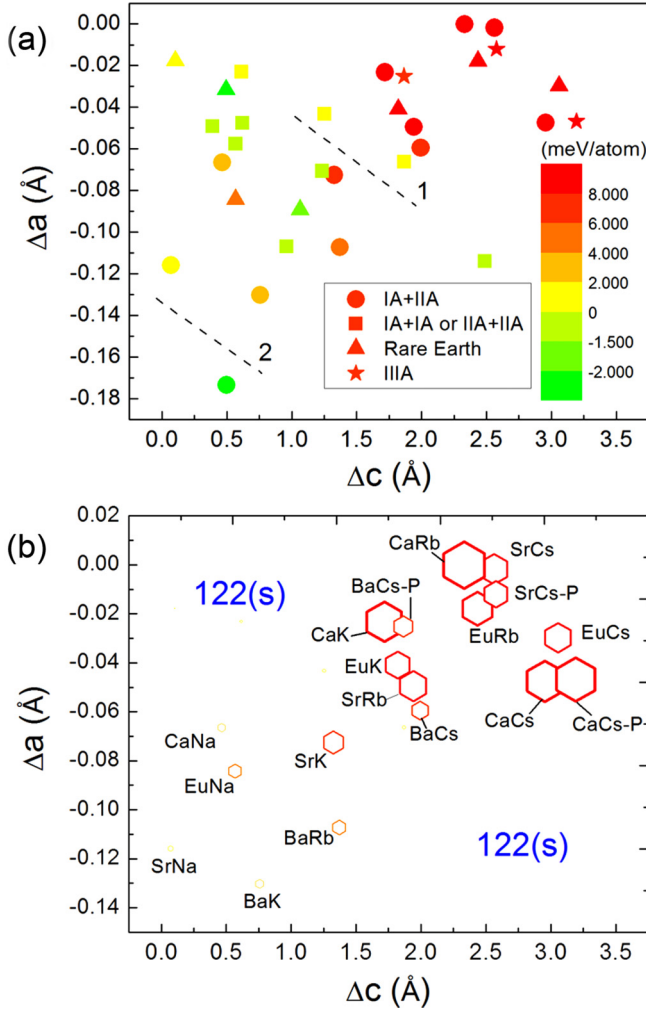


FIG. 6. (a) A generalized phase diagram with new parameters:  $\Delta a = -|a_x - a_y|$ ,  $\Delta c = |c_x - c_y|$ . Defining  $\Delta a$  as negative values is just to give a similar appearance as the original phase diagram [Fig. 2(a)] for easy comparison. The color indicates the value of  $\Delta H$  (meV/atom). Spots above the line 1 are showing  $X$ - $Y$  combinations that have achieved the 1144 phase in experiment. Our calculation shows that the real boundary between 1144 and 122(s) phases is around line 2, which means that combinations between line 1 and line 2 possibly form the 1144-type phase. (b) The stability of various 1144 structures. The size of hexagon is proportional to  $\Delta H$ . Structures with negative  $\Delta H$  not shown. Evidently, the stability increases going from left bottom to right top. In the off-diagonal region, 1144 phase stability is poor, thus it is indicated as 122(s) region.

From Fig. 6(a), two general trends are recognized. First, the stability of the 1144 phase is enhanced as going from the left bottom to the right top. This trend is caused by the size effect as explained with the elastic box picture. Second, IA+IIA combinations (denoted by circles) generally have better 1144 phase stability than IA+IA and IIA+IIA (denoted by squares). This can be seen by comparing square spots with circle spots. Circles have apparently higher  $\Delta H$  than squares, even though their  $\Delta a$  and  $\Delta c$  are similar. Such stability difference is probably relevant to charge transfer: IIA+IIA has one extra electron transferred from cations to Fe-As layers than IA+IIA, while IA+IA has one fewer. Considering the two trends, we

TABLE VI. Lattice constants (obtained from DFT) and enthalpy difference for 1144 phase  $\text{In}X\text{Fe}_4\text{As}_4$ . The last entry is for 122 phase.

Lattice (Å)	$\Delta H$ (meV/atom)	Lattice (Å)	$\Delta H$ (meV/atom)
InCs $a = 3.7694$ $c = 14.5274$	0.243	InBa $a = 3.7882$ $c = 13.7825$	3.802
InRb $a = 3.7433$ $c = 14.2478$	4.072	InSr $a = 3.7920$ $c = 13.2820$	8.283
InK $a = 3.7433$ $c = 13.8952$	4.190	InCa $a = 3.7656$ $c = 12.9925$	12.985
InNa $a = 3.7321$ $c = 13.2495$	1.908	$\text{InFe}_2\text{As}_2$ $a = 3.7240$ $c = 13.8063$	-3.121

are convinced that size effects and charge transfer are two major factors. On the other hand, the magnetic Eu-contained compounds exhibit no abnormality, thus magnetism seems to play a secondary role.

Our calculation provides insight for interpretation of experimental facts. It has been observed that 122(s) and 1144 phases are separated around line 1 in the phase diagram [Fig. 6(a)]. However, in fact, compounds in between line 1 and line 2 [Fig. 6(a)] still energetically favor the 1144 phase, which means the 1144-122(s) phase transition taking place at line 1 is mainly driven by entropy. Thus, compounds between line 1 and line 2 (especially near line 1) possibly form 1144 with a temperature-decreasing annealing process.

Interestingly, IA+IIA with an effective valence state +1.5 generally has lower energy than IA+IA (+1) or IIA+IIA (+2). This suggests that the favorable cation valence state in forming 1144 iron arsenide is +1.5. This might be relevant to the fact that 122 iron arsenide (122 in fact is so similar to 1144) is only found with a cation of +1 or +2 valence states, and no trivalence elements (e.g., La, Ce) have been found. This is probably caused by charge transfer: +1 and +2 are in the neighborhood of energy minimum, while +3 is an overwhelming deviation. Thus, we argue the nonexistence is mainly a consequence of charge effect, instead of size effect. Based on that idea, to stabilize, for instance, the La-contained 1144 structure, one should first consider alkali metals, which will make the effective valence state approach closer to +1.5.

#### IV. CONCLUSION

We find that the 1144 phase can be stabilized in a variety of systems: (i) iron-phosphide  $\text{XYFe}_4\text{P}_4$ , (ii) Eu-contained 1144 iron arsenide  $\text{Eu}X\text{Fe}_4\text{As}_4$ , (iii) indium-contained 1144 compounds  $\text{In}X\text{Fe}_4\text{As}_4$ , suggesting that the 1144 phase is widely existing (see Table VI). The stability of the 1144 phase is summarized in Fig. 6(b). We also show that certain compounds (e.g.,  $\text{BaCsFe}_4\text{As}_4$ ,  $\text{BaRbFe}_4\text{As}_4$ ), which form the 122(s) phase at high temperatures, actually energetically favor the 1144 phase. Thus the 1144 phase is possibly obtained by a well-controlled annealing process.

By analyzing different 1144 systems, we find two factors that intensely affect the stability of the 1144 phase: the mismatch of two building blocks characterized by  $\Delta a$  and  $\Delta c$ , and charge transfer (or the effective valence states of cations).

Based on these findings, the 1144 phase will be stabilized with (i) decreased  $\Delta a$  and increased  $\Delta c$ ; (ii) the cation valence state +1.5. On the other hand, magnetism plays a secondary role. This means that being magnetic would not diminish the chance of obtaining 1144 structures, which paves the way to building rare-earth elements (usually magnetic in nature) into the 1144 phase.

#### ACKNOWLEDGMENTS

The work is inspired by the recent progress in synthesis of the 1144-phase compounds in Paul Canfield's group at Ames

lab. We are very grateful for the enlightening conversation with him. We wish to acknowledge the very helpful discussions with Dr. Canfield, Tai Kong, William Meier, and Ming-yu Xu in the course of doing this work. This work was supported by the US Department of Energy (DOE), Office of Science, Basic Energy Sciences, Materials Science and Engineering Division, including the grant of computer time at the National Energy Research Scientific Computing Center (NERSC) in Berkeley, CA. The research was performed at Ames Laboratory, which is operated for the US DOE by Iowa State University under Contract No. DE-AC02-07CH11358.

- 
- [1] Y. Kamihara, T. Watanabe, M. Hirano, and H. Hosono, *J. Am. Chem. Soc.* **130**, 3296 (2008).
- [2] A. Iyo, K. Kawashima, T. Kinjo, T. Nishio, S. Ishida, H. Fujihisa, Y. Gotoh, K. Kihou, H. Eisaki, and Y. Yoshida, *J. Am. Chem. Soc.* **138**, 3410 (2016).
- [3] Y. Liu, Y. B. Liu, Z.-T. Tang, H. Jiang, Z.-C. Wang, A. Ablimit, W. H. Jiao, Q. Tao, C. M. Feng, Z. A. Xu, and G. H. Cao, *Phys. Rev. B* **93**, 214503 (2016).
- [4] K. Kawashima, T. Kinjo, T. Nishio, S. Ishida, H. Fujihisa, Y. Gotoh, K. Kihou, H. Eisaki, Y. Yoshida, and A. Iyo, *Phys. Soc. Jpn.* **85**, 064710 (2016).
- [5] W. R. Meier, T. Kong, U. S. Kaluarachchi, V. Taufour, N. H. Jo, G. Drachuck, A. E. Böhmer, S. M. Saunders, A. Sapkota, A. Kreyssig, M. A. Tanatar, R. Prozorov, A. I. Goldman, F. F. Balakirev, A. Gurevich, S. L. Bud'ko, and P. C. Canfield, *Phys. Rev. B* **94**, 064501 (2016).
- [6] Y. Liu, Y.-B. Liu, Q. Chen, Z.-T. Tang, W.-H. Jiao, Q. Tao, Z.-A. Xu, and G.-H. Cao, *Sci. Bull.* **61**, 1213 (2016).
- [7] W. R. Meier, T. Kong, S. L. Bud'ko, and P. C. Canfield, *Phys. Rev. Materials* **1**, 013401 (2017).
- [8] P. K. Biswas, A. Iyo, Y. Yoshida, H. Eisaki, K. Kawashima, and A. D. Hillier, *Phys. Rev. B* **95**, 140505(R) (2017).
- [9] K. Cho, A. Fente, S. Teknowijoyo, M. A. Tanatar, K. R. Joshi, N. M. Nusran, T. Kong, W. R. Meier, U. Kaluarachchi, I. Guillamon, H. Suderow, S. L. Bud'ko, P. C. Canfield, and R. Prozorov, *Phys. Rev. B* **95**, 100502(R) (2017).
- [10] R. Yang, Y. Dai, B. Xu, W. Zhang, Z. Qiu, Q. Sui, C. C. Homes, and X. Qiu, *Phys. Rev. B* **95**, 064506 (2017).
- [11] D. Mou, T. Kong, W. R. Meier, F. Lochner, L.-L. Wang, Q. Lin, Y. Wu, S. L. Bud'ko, I. Eremin, D. D. Johnson, P. C. Canfield, and A. Kaminski, *Phys. Rev. Lett.* **117**, 277001 (2016).
- [12] K. Sasmal, B. Lv, B. Lorenz, A. M. Guloy, F. Chen, Y.-Y. Xue, and C.-W. Chu, *Phys. Rev. Lett.* **101**, 107007 (2008).
- [13] G. Wu, H. Chen, T. Wu, Y. L. Xie, Y. J. Yan, R. H. Liu, X. F. Wang, J. J. Ying, and X. H. Chen, *J. Phys.: Condens. Matter* **20**, 422201 (2008).
- [14] K. Zhao, Q. Q. Liu, X. C. Wang, Z. Deng, Y. X. Lv, J. L. Zhu, F. Y. Li, and C. Q. Jin, *J. Phys.: Condens. Matter* **22**, 222203 (2010).
- [15] D. M. Wang, X. C. Shangguan, J. B. He, L. X. Zhao, Y. J. Long, P. P. Wang, and L. Wang, *J. Supercond. Novel Magn.* **26**, 2121 (2013).
- [16] N. Shinohara, K. Tokiwa, H. Fujihisa, Y. Gotoh, S. Ishida, K. Kihou, C. H. Lee, H. Eisaki, Y. Yoshida, and A. Iyo, *Supercond. Sci. Technol.* **28**, 062001 (2015).
- [17] S. Sharma, A. Bharathi, S. Chandra, V. R. Reddy, S. Paulraj, A. T. Satya, V. S. Sastry, A. Gupta, and C. S. Sundar, *Phys. Rev. B* **81**, 174512 (2010).
- [18] N. Barisic, D. Wu, M. Dressel, L. J. Li, G. H. Cao, and Z. A. Xu, *Phys. Rev. B* **82**, 054518 (2010).
- [19] S. Jiang, H. Xing, G. Xuan, C. Wang, Z. Ren, C. Feng, J. Dai, Z. Xu, and G. Cao, *J. Phys.: Condens. Matter* **21**, 382203 (2009).
- [20] Z.-C. Wang, C.-Y. He, S.-Q. Wu, Z.-T. Tang, Y. Liu, A. Ablimit, Q. Tao, C.-M. Feng, Z.-A. Xu, and G.-H. Cao, *J. Phys.: Condens. Matter* **29**, 11LT01 (2017).
- [21] A. Togo and I. Tanaka, *Scr. Mater.* **108**, 1 (2015).
- [22] G. Kresse and J. Furthmüller, *Comput. Mater. Sci.* **6**, 15 (1996).
- [23] J. P. Perdew, K. Burke, and M. Ernzerhof, *Phys. Rev. Lett.* **78**, 1396 (1997).
- [24] P. E. Blochl, *Phys. Rev. B* **50**, 17953 (1994).
- [25] H. S. Jeevan, D. Kasinathan, H. Rosner, and P. Gegenwart, *Phys. Rev. B* **83**, 054511 (2011).
- [26] Y. Tokiwa, S. H. Hubner, O. Beck, H. S. Jeevan, and P. Gegenwart, *Phys. Rev. B* **86**, 220505 (2012).
- [27] A. I. Goldman, D. N. Argyriou, B. Ouladdiaf, T. Chatterji, A. Kreyssig, S. Nandi, N. Ni, S. L. Bud'ko, P. C. Canfield, and R. J. McQueeney, *Phys. Rev. B* **78**, 100506(R) (2008).
- [28] I. Nowik, I. Felner, Z. Ren, G. H. Cao, and Z. A. Xu, *J. Phys.: Condens. Matter* **23**, 065701 (2011).
- [29] H. S. Jeevan, Z. Hossain, D. Kasinathan, H. Rosner, C. Geibel, and P. Gegenwart, *Phys. Rev. B* **78**, 052502 (2008).
- [30] Y. Xiao, Y. Su, W. Schmidt, K. Schmalzl, C. M. N. Kumar, S. Price, T. Chatterji, R. Mittal, L. J. Chang, S. Nandi, N. Kumar, S. K. Dhar, A. Thamizhavel, and T. Brueckel, *Phys. Rev. B* **81**, 220406(R) (2010).
- [31] A. I. Coldea, C. M. J. Andrew, J. G. Analytis, R. D. McDonald, A. F. Bangura, J.-H. Chu, I. R. Fisher, and A. Carrington, *Phys. Rev. Lett.* **103**, 026404 (2009).
- [32] P. J. W. Moll, J. Kanter, R. D. McDonald, F. Balakirev, P. Blaha, K. Schwarz, Z. Bukowski, N. D. Zhigadlo, S. Katrych, K. Mattenberger, J. Karpinski, and B. Batlogg, *Phys. Rev. B* **84**, 224507 (2011).
- [33] E. Razzoli, C. E. Matt, M. Kobayashi, X.-P. Wang, V. N. Strocov, A. van Roekeghem, S. Biermann, N. C. Plumb, M. Radovic, T. Schmitt, C. Capan, Z. Fisk, P. Richard, H. Ding, P. Aebi, J. Mesot, and M. Shi, *Phys. Rev. B* **91**, 214502 (2015).
- [34] Z.-C. Wang, C.-Y. He, S.-Q. Wu, Z.-T. Tang, Y. Liu, and G.-H. Cao, *Chem. Mater.* **29**, 1805 (2017).
- [35] S.-Q. Wu, Z.-C. Wang, C.-Y. He, Z.-T. Tang, Y. Liu, and G.-H. Cao, *Phys. Rev. Materials* **1**, 044804 (2017).
- [36] H. Katsuraki and K. Suzuki, *J. Appl. Phys.* **36**, 1094 (1965).